https://doi.org/10.5194/egusphere-2026-4081
Preprint. Discussion started: 4 August 2026

Windstorms in a Warming Climate: Urban Flow Dynamics, Climate Change, and Future Extremes

Johanne Kristine Haandbæk Øelund[1, 2, 3, 4], Jens Hesselbjerg Christensen[1], Amalie Renée Hartvig Jensen[3], and Hans Holger Hundborg Koss[3]

[1]University of Copenhagen, Section for the Physics of Ice, Climate and Earth, Niels Bohr Institute, Copenhagen, Denmark
[2]DMI - Danish Meteorological Institute, Copenhagen, Denmark
[3]DTU Construct, Lyngby, Denmark
[4]DTU Management, Lyngby, Denmark

Correspondence: Johanne Kristine Haandbæk Øelund (johanne.oelund@nbi.ku.dk)

Abstract. This study explores how intensified large-scale storm forcing translates into urban-scale wind exposure in a dense historical urban environment using high-resolution large-eddy simulations (LES) with the PALM-4U model. A realistic representation of central Copenhagen is subjected to a series of idealised inflow wind conditions with progressively stronger storm scenarios, ranging from weak to severe wind forcing.

To estimate the influence of mesoscale weather variations due to a change in climatic boundary conditions on the wind field of the built environment, the study introduces and demonstrates a novel statistical wind flow analysis across horizontal layers of the computational domain.

As expected from urban canopy theory the results show that the spatial organisation of the flow field remains largely invariant across all simulations, indicating that urban morphology governs the structure of the wind field, while inflow speed primarily controls the magnitude of the mean response, but here confirmed qualitatively across a wide range of forcing conditions.

In contrast gust characteristics exhibit strongly wind speed-dependent behaviour. At low inflow wind speeds, gustiness is strongly enhanced by intermittent and geometry-driven recirculation processes within the urban canopy, resulting in elevated turbulence intensity and gust factors. At higher inflow wind speeds, both turbulence intensity and gust factors converge toward quasi-stationary values, indicating a transition to a shear-dominated canopy flow in which gust amplification decreases and extreme events scale more proportionally with the mean flow.

These findings demonstrate that urban wind hazards under intensified storm conditions cannot be assessed from mean wind scaling alone, as gust amplification is governed by non-linear interactions between turbulent structures and urban geometry that are most pronounced at low-to-moderate inflow wind speeds. The study provides a physically based framework for understanding how changes in inflow wind intensity map to different wind hazard metrics in complex urban environments, explicitly distinguishing between mean-flow scaling and turbulence-driven amplification of gusts.

https://doi.org/10.5194/egusphere-2026-4081
Preprint. Discussion started: 4 August 2026

1 Introduction

Over the past decades, increasing attention has been devoted to understanding how human activities influence the global climate system, (e.g. IPCC, 2021, 2022). While the long-term increase in global mean temperature is well established, significant uncertainties remain regarding how a warmer climate will influence atmospheric circulation and extreme weather systems.

Extratropical windstorms in the North Atlantic–European sector are governed by the interaction between large-scale atmospheric circulation, baroclinic development, and transient eddy dynamics (Hoskins and Hodges, 2002; Ulbrich et al., 2009; Catto, 2016; Priestley and Catto, 2022), with storm intensity and structure strongly modulated by both thermodynamic and dynamical processes (Catto et al., 2019; Büeler and Pfahl, 2017). Recent studies indicate that climate change may intensify mid-latitude storms, potentially leading to stronger near-surface wind fields over Northern Europe. High-resolution regional climate simulations of historical extreme events suggest that storms occurring in a warmer climate may exhibit increased wind intensity, longer duration, and larger spatial extent. For example, simulations of the storm that struck Denmark in December 1999 have shown that the event could become substantially more intense under warmer climate conditions (Øelund et al., 2026; Zeitzen et al., 2025). Similar findings (e.g. Hawkins et al., 2023; Ermis et al., 2024) have been reported for other extratropical storms, suggesting that future wind hazards may increase in both magnitude and spatial impact.

While such studies provide valuable insight into large-scale atmospheric processes, they do not resolve the spatial scales at which wind affects people, buildings, and infrastructure, particularly within cities, where exposure is more concentrated and consequences most acute. Mesoscale atmospheric models typically operate at grid resolutions ranging from hundreds of metres to several hundred kilometres, which is considerably larger than the characteristic length scales of urban features such as buildings, street canyons, and individual obstacles. Consequently, they cannot explicitly resolve the complex flow interactions that occur within dense urban environments, including flow separation, recirculation, and turbulence generated by buildings. Instead, urban processes must be parameterised, introducing significant uncertainty in estimates of local wind exposure (Nazarian et al., 2020).

A long-standing challenge in wind engineering and urban climatology is therefore the scale gap between mesoscale atmospheric modelling and the microscale flow processes that occur within complex urban environments. Urban morphology significantly modifies atmospheric flow through channelling, acceleration, recirculation, and wake formation, creating highly heterogeneous wind fields within cities (Blocken, 2015). Consequently, the relationship between large scale wind forcing and local wind exposure is not straightforwardly proportional. While spatially averaged mean flow tends to scale roughly linearly with inflow wind speed, localised gust amplification is strongly mediated by urban geometry and building configuration, showing non-linearity in the extremes (Fernando, 2010).

Understanding how intensified storm forcing manifests at the human scale therefore requires high-resolution modelling approaches capable of resolving urban flow structures. Large-eddy simulation (LES) models have emerged as powerful tools for this purpose, as they explicitly resolve turbulent flow structures and enable detailed representation of the flow patterns around complex urban geometry (Blocken, 2015; Fernando, 2010; Maronga et al., 2020). When combined with detailed urban geometry, LES models allow investigation of how background wind forcing interacts with buildings and street networks to

https://doi.org/10.5194/egusphere-2026-4081
Preprint. Discussion started: 4 August 2026

produce localised wind accelerations and turbulent structures. The LES based urban climate model PALM-4U is a state-of-the-art modelling framework developed for high-resolution simulations of atmospheric flow in complex urban environments (Maronga et al., 2020).

The question of how intensified storm forcing translates to local urban wind conditions becomes increasingly relevant in the context of climate change (Priestley et al., 2024). If extratropical storms intensify in a warmer climate (Øelund et al., 2026; Hawkins et al., 2023), enhanced background wind forcing may interact with urban morphology in ways that increase local wind amplification, particularly through gust enhancement at low to moderate inflow wind speeds, and thereby elevate wind-related risk. The urban environment translates the approaching wind in different ways into the open space between buildings. Dense and irregular street patterns generally provide high shelter effects. However, some configurations like singular buildings elevating significantly above the surrounding development (downwash effect), or wide streets or places narrowing to smaller passages (funnel effect) can lead to local high wind exposure at pedestrian level.

A key question is therefore whether this amplification acts primarily on mean wind speeds, on gust or differently across the inflow wind speed range, distinctions with direct implications for wind hazard assessment under future storm conditions.

In this study, the scale gap between large-scale storm forcing and urban wind exposure is explored by investigating the response of a dense historical urban district in central Copenhagen to progressively intensified background wind forcing. Using the LES-based urban climate model PALM-4U (Maronga et al., 2020), a high-resolution representation of the area surrounding Greyfriar Square (Gråbrødretorv) is subjected to a series of idealised inflow scenarios spanning a wide range of wind velocities and two wind directions, representing potential future storm conditions in a warmer climate. The aim is to quantify how large-scale inflow wind speed translates into spatially averaged mean flow and extreme near-surface gusts within the urban canopy, and specifically whether these two quantities scale differently with the inflow forcing. The idealised inflow profiles used here represent a first step toward the longer-term goal of driving PALM-4U directly with large-scale meteorological model output, a coupling not yet achieved in the present study.

The study addresses three main questions:

1. How does increasing large-scale wind forcing translate into local wind fields within a dense historical urban environment?
2. Does gust amplification by urban geometry exhibit non-linear dependence on inflow wind speed, and if so, over what range of wind forcing does this behaviour occur?
3. Do the simulated flow fields exhibit physically consistent behaviour across the full range of storm-strength wind forcing, and thereby supporting the use of PALM-4U as a tool for urban wind hazard assessment?

By combining physically self-consistent but idealised inflow profiles with detailed urban geometry, the study provides new insight into how intensified extratropical storm conditions may manifest at the human scale, offering a first step toward a framework linking large-scale storm intensity to local urban wind hazard.

https://doi.org/10.5194/egusphere-2026-4081
Preprint. Discussion started: 4 August 2026

2 Methodology

2.1 Study area - medieval Copenhagen

The computational domain is built around Greyfriar Square, centred in the historical inner city of Copenhagen (see Figure 1). The street network is very dense and irregular with narrow street canyons and heterogeneous building heights, which create a highly complex urban morphology. The area includes the square, old historical buildings dating back to 1730's and 1800's, the church of the holy ghost (Helligånds kirken) and part of the shopping street (Bramsen and Fogtdal, 1997). Dense and irregular urban environments can strongly modify the incoming atmospheric flow through interactions with buildings and street networks. Rather than promoting uniform wind channelling, narrow and irregularly oriented streets can lead to complex flow patterns involving local acceleration, sheltering effects, recirculation zones, and enhanced turbulence. Such environments therefore provide a suitable test case for investigating localized wind amplification under strong wind conditions.

Figure 1. Overview of the model domain and sub-domains. The inset map (top left) shows the location within Denmark (left). The main map (right) shows the model domains over Copenhagen: The horizontal boundaries of the computational domain are illustrated with a grey square, constituting the parent domain which includes the urban area within the blue circle. The first child domain is marked in yellow, and the second child domain in green, where most of the analyses were carried out. The red dot in the centre indicates the location of Greyfriar Square, where virtual measurements were carried out.

2.2 Palm-4U: Model description

Numerical simulations were conducted using the PALM-4U model system, a high-resolution large-eddy simulation framework designed for urban environments (Maronga et al., 2020). PALM-4U explicitly resolves turbulence structures and incorporates three-dimensional urban geometry, using cubic grid blocks at the resolution of the finest computational grid, enabling physically

https://doi.org/10.5194/egusphere-2026-4081
Preprint. Discussion started: 4 August 2026

consistent representation of flow channelling, acceleration, and wake formation within complex urban domains. This Cartesian representation necessarily simplifies curved or angled building façades into a stepped approximation, with geometric fidelity increasing at finer grid spacing. The model has previously been applied to studies of urban climate, wind flow, and pollutant dispersion, demonstrating its capability to capture microscale flow processes influenced by urban morphology (e.g. Belda et al., 2021; Resler et al., 2024).

The PALM model system has frequently been applied to studies of urban climate, urban heat islands, and pollutant dispersion, in which wind fields have primarily served as a means of model validation rather than as the primary subject of investigation (e.g. Resler et al., 2021; Kiseleva et al., 2024). In contrast, the present study focuses specifically on the performance of PALM-4U under strong wind conditions representative of storm events.

The computational model domain has a total lateral extension of 2048 m x 2048 m and domain height of 512 m, with Greyfriar Square located approximately in the domain centre. The one-way self-nesting feature of PALM (Hellsten et al., 2021) was used to gradually refine the grid resolution towards the area of interest. This was achieved by adding two nested computational sub-domains (child domains) embedded in each other and horizontally centred in the model as displayed in Figure 1 and Appendix A. Consequently, the grid resolution increases from 8 m to 4 m and finally to 1 m from the outermost domain (parent) to the innermost domain (second child). Within each (sub-)domain, the Cartesian grid is structured with equidistant spacing in both horizontal and vertical directions. The first child domain extend 768 x 768 m with a height of 256 m and the second child domain extend 256 x 256 m with a height of 128 m.

The building height of the inner child 2 is shown in Figure 2. The red dashed line marks the transect through Greyfriar Square, which coincides with the centre of the model domain and the location of the virtual measurement point; the green dotted line marks the transect through the churchyard, adjacent to the church of the holy ghost, visible in the figure as the building cluster at approximately (x, y) ≈ (75, 25) m.

The topography model, containing both buildings and orography, is illustrated in Appendix B. It aims to represent realistic conditions of the area and distinguishes between different key surface types (buildings, soil/green/paved areas, and water masses) for surface-atmosphere exchange processes. However, its representation is constrained by PALM's Cartesian grid structure and user-defined local grid sizes. Additional simplifications of the surface geometry were introduced to reduce computational demand while maintaining the overall characteristics of the study area.

2.3 Model simulation setup

A series of simulations was conducted with prescribed logarithmic inflow wind profile with velocities of: $5, 10, 15, 20, 25, 30$ and 35 ms^{-1} in 10 m height. A 3.48 ms^{-1} at 10 m height was also carried out for comparison with in-situ data.

The inflow wind direction was set to South-South-West (SSW) to allow validation against available measurements. An additional simulation with a westerly (W) wind direction was performed to assess the influence of wind direction on the simulated flow for 25 ms^{-1}.

https://doi.org/10.5194/egusphere-2026-4081
Preprint. Discussion started: 4 August 2026

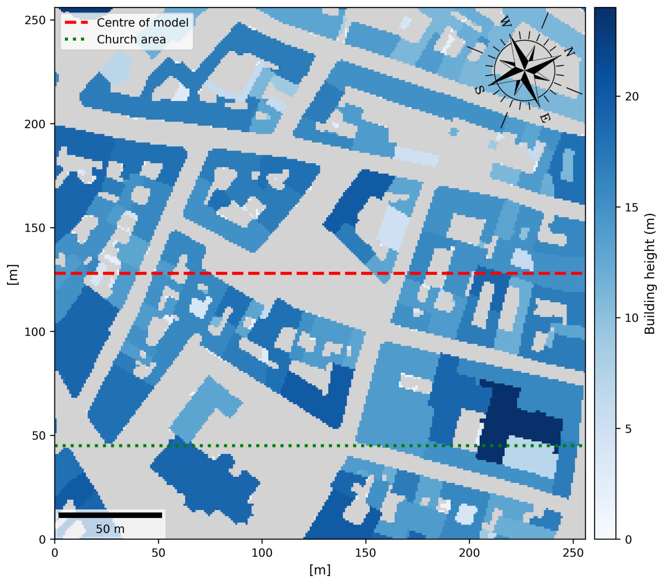

Figure 2. Building height distribution within the nested model domain Child 2. Building height is indicated by a blue colour gradient, with darker shades representing taller buildings. The red dashed line and green dotted line show the locations of the cross-sections extracted from the model results.

Each simulation consisted of:

- A soil/wall spin-up period of 3 hours (thermal spin-up for the model's soil and wall layers), followed by an additional 1 hour and 10 min spin-up for the wind and turbulence.
- A subsequent 1-hour simulation period used for analysis.

The wind spin-up duration was chosen to allow the development of dynamically balanced turbulence structures and to ensure statistical stationarity prior to analysis. All statistical quantities presented in this study were computed using data from the last 1 hour period.

2.4 Boundary conditions and wind forcing

A horizontally homogeneous initial state was prescribed, defined by piecewise linear vertical profiles of temperature, humidity, and horizontal wind speed at the inflow boundary, specified at 8 m vertical intervals consistent with the parent domain grid spacing. The wind profile was calculated using the log-law formula:

$$v_2 = v_1 \frac{\ln\left(\frac{h_2}{z_0}\right)}{\ln\left(\frac{h_1}{z_0}\right)} \qquad (1)$$

https://doi.org/10.5194/egusphere-2026-4081
Preprint. Discussion started: 4 August 2026

Boundary conditions were identical across all simulations except for the imposed inflow wind speed and pressure gradient along the computational domain, thereby identifying the sensitivity of flow characteristics to wind forcing magnitude.

The horizontal pressure gradient driving the flow was derived from the friction velocity u_*, calculated from the prescribed inflow wind speed at 10 m reference height:

$$u_* = \frac{U(z)\kappa}{\ln \frac{z}{z_0}}, \tag{2}$$

The corresponding horizontal pressure gradient was then obtained as:

$$\frac{1}{\rho}\frac{\partial p}{\partial x} \approx \frac{u_*^2}{H} \Rightarrow dpdx \approx -\rho \frac{u_*^2}{H} \tag{3}$$

2.5 Model consistency check

A single low-wind-speed case (3.48 $\mathrm{m\,s^{-1}}$ at 10 m height) was compared qualitatively against in-situ wind measurements collected at the centre of Greyfriar Square, Copenhagen, during summer 2018. The measurements were obtained using a Kestrel Heat Stress Tracker with a sampling frequency of 0.5 Hz over a single 10-minute period and at a single point at pedestrian level (1.5 m). The measurements' limited spatial and temporal coverage introduces considerable uncertainty when used as validation data, both in terms of representativeness of mean conditions and in terms of instrument accuracy for field deployment.

The observed 10-minute mean wind speed at pedestrian level was 2.53 $\mathrm{m\,s^{-1}}$, compared to 2.51 $\mathrm{m\,s^{-1}}$ in the PALM-4U simulation. While this close agreement is encouraging, it should not be over-interpreted: the comparison involves only a single point, a single short observational period, and a weak-wind regime that may not be representative of the turbulent dynamics investigated in this study.

This check is therefore not intended as a model validation in any formal sense. It provides only a basic order-of-magnitude indication that the model configuration and urban setup do not produce grossly unrealistic mean flow magnitudes under weak wind conditions. The absence of independent validation data for stronger wind cases represents a limitation of the present study, and the results should be interpreted accordingly (Jensen and Koss, 2026; Thordal et al., 2020).

2.6 Data Analysis

Figure 3 illustrates the main elements in the vertical structure of urban wind flow. Here, the flow in the urban canopy layer consists of three zones: the pedestrian layer at the bottom followed by a recirculation dominated zone above and on top the separation flow field at average building height. A transition zone connects the urban canopy layer with the free wind aloft, which is assumed to be unaffected by the urban morphology.

This study focuses on the building-height and canopy-level regimes, where urban morphology most directly modifies the approaching wind.

Output from the simulations was analysed to quantify how the wind field approaching the urban area, represented by the prescribed inflow wind speed, is modified by urban geometry as it enters and moves through the urban canopy, and how

https://doi.org/10.5194/egusphere-2026-4081
Preprint. Discussion started: 4 August 2026

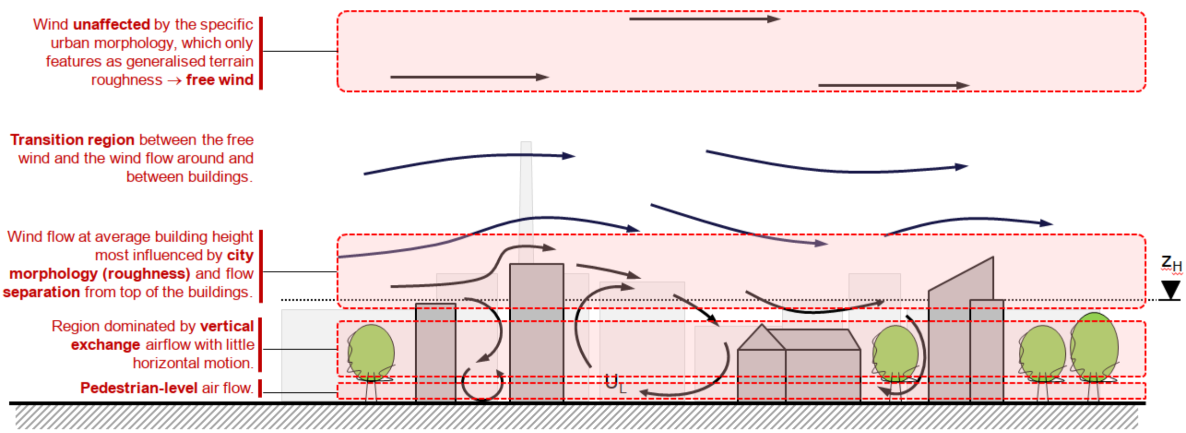

Figure 3. Expected characteristics flow regions in the urban boundary layer. Figure inspired by Oke (1984)

the degree of this modification scales with increasing inflow wind speed. The primary objective is to relate the imposed inflow wind forcing to spatially averaged mean wind conditions within the urban canopy and to the occurrence of extreme near-surface gusts, as a step toward the longer-term goal of linking large-scale storm intensity to local urban wind hazard.

Two complementary analyses were performed.

First, the speed-up factor was computed at every grid point within the Child 2 domain, generating a spatial speed-up factor used to assess the spatial heterogeneity of wind amplification, that is, how the ratio of local wind speed to inflow velocity varies across the domain, identifying urban configurations and flow structures associated with locally enhanced wind exposure. This grid-point analysis uses the full 1-hour simulation period, but does not isolate gust. It is therefore treated as an approximate, spatially resolved amplification metric rather than an engineering gust factor.

Second, mean wind speed, turbulence intensity, and a fully resolved gust factor were computed at a virtual measurement point located at the centre of Greyfriar Square (Centred red dot Figure 1), used for the scaling analysis presented in the results.

For each simulation, the following quantities were evaluated at the virtual measurement point: mean wind speed, turbulence intensity, power spectral density, and gust factor.

Together, these diagnostics are used to investigate the relationship between imposed inflow velocity, spatially averaged mean flow, and extreme gust response within the urban canopy, specifically, whether the ratio between gust and mean wind speed, and between turbulence intensity and mean wind speed, remains constant or varies systematically with increasing inflow forcing, as presented in Section 2.4.

Turbulence intensity, denoted I_u following standard wind engineering convention, is defined as $I_u = \frac{\sigma_u}{\bar{u}}$, where σ_u denotes the standard deviation of the stream wise wind speed component and $\bar{u}$ is the mean wind speed.

The gust factor is defined as $G = \frac{u_{max}}{\bar{u}}$, where u_{max} denotes the maximum wind speed.

Both u_{max} and $\bar{u}$ are computed for two areas of interest: the full Child 2 domain (green boundary in Figure 1), where u_{max} is taken as the maximum wind speed in the entire child 2 over the full 1-hour simulation period, and the virtual measurement

https://doi.org/10.5194/egusphere-2026-4081
Preprint. Discussion started: 4 August 2026

point at the centre of Greyfriar Square (red dot in Figure 1), where u_{max} is defined as the maximum 3-second gust within a 10-minute window (Davis and Newstein, 1968), evaluated across the full 1-hour dataset. These two definitions and areas of interest are used consistently throughout the analysis.

To characterise the height-dependent relationship between inflow velocity and local wind response, the mean wind speed at each height level within Child 2 was evaluated as a function of the imposed inflow velocity, for all seven inflow speeds. The resulting set of response curves, termed the urban flow transfer function (UFT-function), describes how wind speed at a given height responds to changes in the imposed background forcing, relative to the unchanged-flow case in which local wind speed equals the inflow velocity. The UFT-function is used in Section 3 to identify the characteristic vertical flow regions: Free flow, transition layer, rooftop separation, recirculation, and pedestrian level, through which the simulated wind response passes as height decreases from the free atmosphere to the ground.

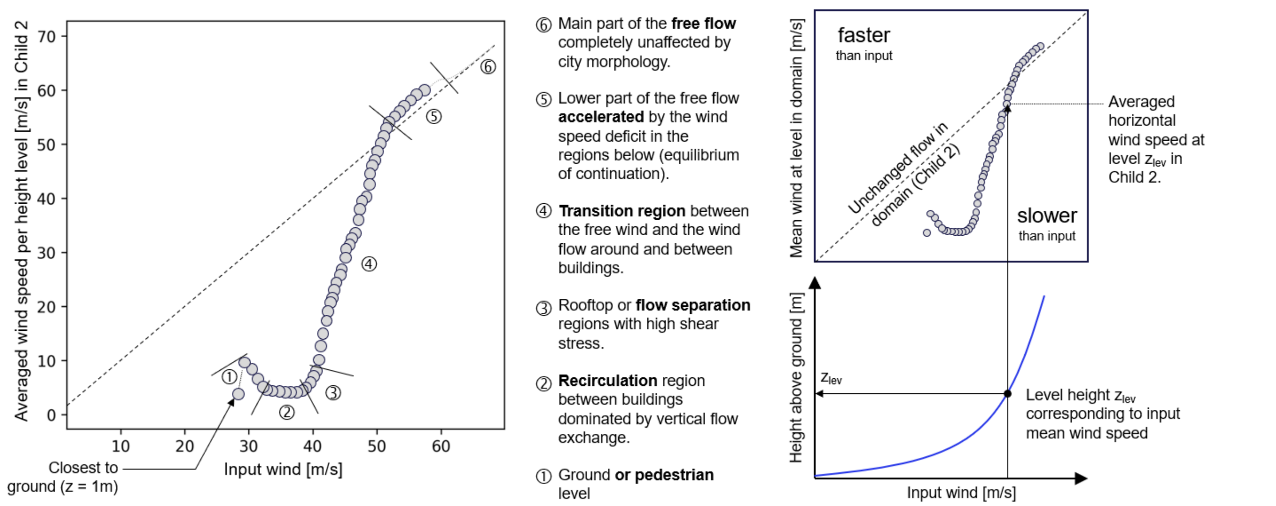

Figure 4. Reading the characteristic of the urban flow transfer function.

Figure 4 presents the UFT-function schematically, with the six flow regions explicitly numbered and described: (1) the upper free flow, unaffected by city morphology; (2) the lower free flow, locally accelerated by the wind speed deficit in the layers below; (3) the transition region between free flow and the wind flow around and between buildings; (4) the rooftop or flow separation region, characterised by high shear; (5) the recirculation region between buildings, dominated by vertical flow exchange; and (6) the ground or pedestrian level. A dashed line marking unchanged flow (where local wind speed equals the inflow value) shows that the lower free-flow region is consistently faster than the inflow, while the canopy region remains consistently slower, a direct visual summary of the amplification and attenuation behaviour described throughout this section.

2.7 Assumptions and Limitations

While the inflow conditions are idealised rather drawn directly from meteorological model output, the use of physically selfconsistent logarithmic profiles spanning a wide range of wind speeds ensures that the simulated flow fields are dynamically

https://doi.org/10.5194/egusphere-2026-4081
Preprint. Discussion started: 4 August 2026

representative of the boundary layer conditions associated with extratropical storm events. The results can therefore be interpreted in terms of how large-scale storm intensification, as projected under future climate conditions, translate into urban wind exposure (Øelund et al., 2026). The focus on mean and gust wind speeds within the urban canopy provides a first order characterisation of how large scale storm forcing manifests at local scale.

The child domains use a horizontal grid spacing of 4 and 1 m respectively, nested within an 8 m parent domain, resulting in a refinement ratio of 8:4:1. Previous studies using PALM typically recommend ratios of 2–4 to minimise interpolation errors at the nesting interface (Hellsten et al., 2021).

3 Results

Figure 5 presents the spatial distribution of the 10-minute mean wind speed at approximately 10 m height for selected inflow wind speeds between 5 to 35 ms^{-1}. The overall flow pattern remains similar, with the strongest wind speeds occurring in the same area within Child 2, across all simulations. This suggests that the principal flow structures within the urban area are spatially anchored by building geometry rather than by the magnitude of the approaching wind, though a quantitative assessment of this similarity would require a normalised colour scale across panels, which is left for future analysis.

Speed-up areas of elevated wind speed are consistently observed in the open space immediately downstream of the church and within the narrow streets aligned with the inflow direction. In contrast, locations with reduced wind speeds occur typically in sheltered regions located behind buildings and in streets oriented perpendicular to the approaching flow. As the inflow wind speed increases, the local wind speeds increase throughout the domain while preserving the overall spatial distribution.

To quantify this behaviour, the domain-averaged and domain-maximum wind speeds were evaluated as functions of the imposed inflow velocity. Both quantities exhibited a strong linear relationship with the inflow conditions, yielding coefficients of determination of $R^2 = 0.9864$ and $R^2 = 0.9855$ for the mean and maximum wind speeds, respectively (see appendix C). These results confirm that the local wind field responds approximately linearly to the imposed inflow velocity over the investigated range.

Although the spatial distribution of the mean wind speed remains similar across all simulations, the temporal evolution of the wind field reveals important differences. Figure 6 shows the domain-averaged (the spatial average of wind speed across all grid points within Child 2 at 10 m height) and domain-maximum (the single highest wind speed occurring anywhere within Child 2 at 10 m height) wind speeds during the analysed period. The domain-averaged wind speeds exhibit a nearly proportional increase with inflow velocity and maintain a similar temporal evolution, consistent with the approximately linear scaling observed in the spatial analysis.

In contrast, the domain-maximum wind speeds display a more irregular behaviour. While the magnitude of the maximum wind speed generally increases with increasing inflow velocity, peak events do not occur simultaneously across the simulations. As only a single realisation was simulated for each inflow speed, this misalignment cannot be distinguished from the expected stochastic variability of turbulent gusts and should not, on this basis alone, be interpreted as evidence of inflow-velocity-

https://doi.org/10.5194/egusphere-2026-4081
Preprint. Discussion started: 4 August 2026

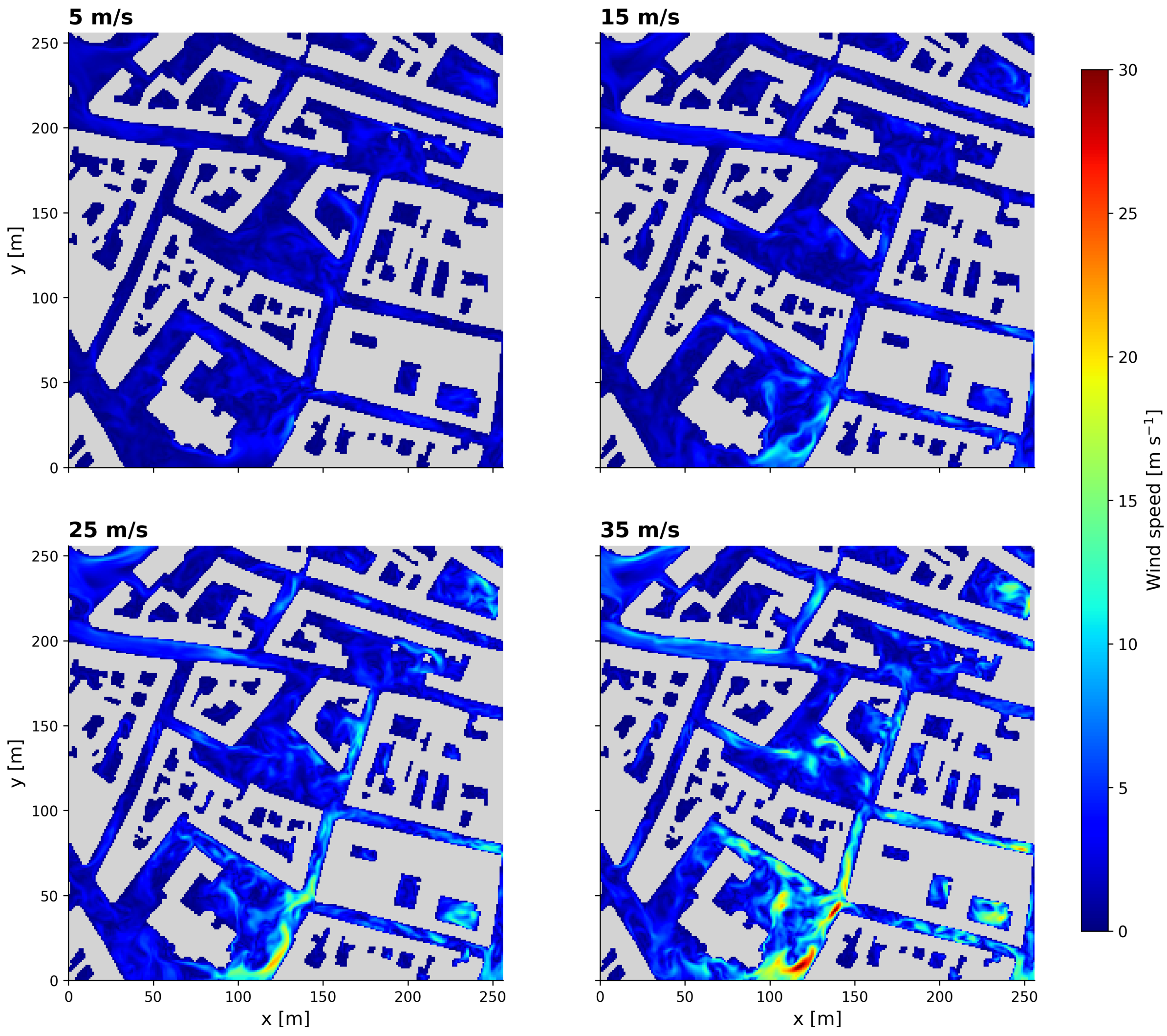

Figure 5. Distribution of the resulting horizontal wind speed in a plane 10 m above ground level in Child 2 domain for selected inflow wind speeds $\bar{U}_{10}$.

https://doi.org/10.5194/egusphere-2026-4081
Preprint. Discussion started: 4 August 2026

dependent turbulent structure. It does, however, indicate that the strongest local gusts at a given moment in time are not simply time-synchronised, scaled versions of the inflow forcing.

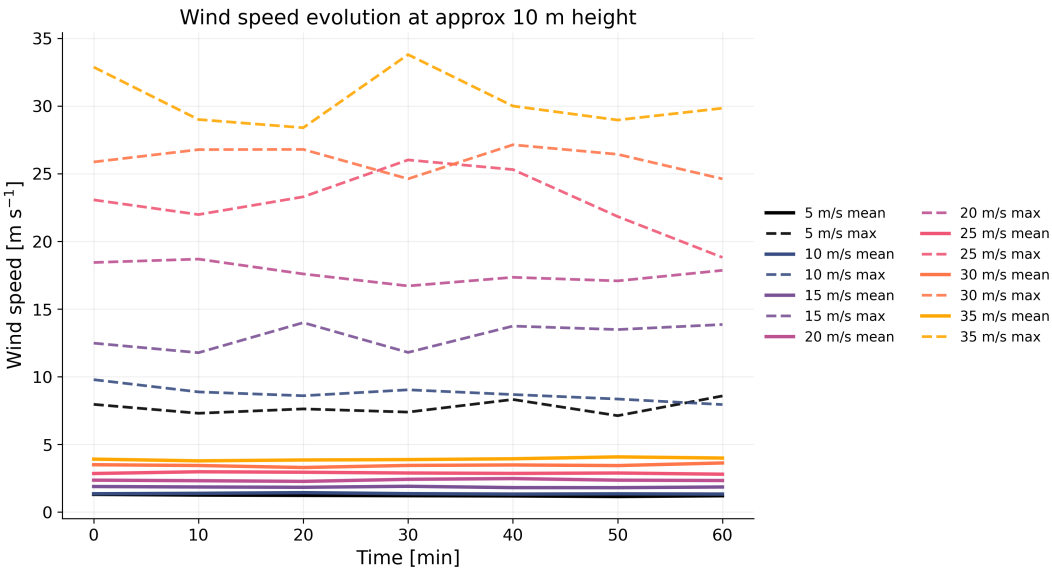

Figure 6. Temporal development of the mean (full line) and maximum wind speed (dashed line) over a 1-hour period within the Child 2 domain for each model run.

Vertical cross-sections through the computational domain (Figures 7 and 8) illustrate the mean flow structure within and above the urban canopy, using a fixed colour scale (0–30 m s^{-1} across all panels). Within the canopy layer, the spatial pattern of recirculation and wake structures remains largely consistent across the full range of inflow velocities, supporting the interpretation that canopy-scale flow structure is primarily governed by urban geometry. Above the canopy, wind speed increases visibly with inflow velocity at low to moderate forcing (panels a–c); at higher inflow velocities (panels d–g, $\geq 20ms^{-1}$), the free-stream wind speed exceeds the upper bound of the colour scale, and absolute magnitude differences between these higher-speed simulations are therefore not visually distinguishable in this figure. This behaviour is broadly consistent with the approximately linear scaling of mean wind speed with inflow velocity described above.

The cross-section through Greyfriar Square (Figure 7) reveals substantial spatial variability in the mean wind field. Accelerated wind speeds occur above rooftop level and within open areas aligned with the approaching flow, whereas lower wind speeds are observed in sheltered regions between buildings. Strong velocity gradients are present near rooftop height, indicating a transition between the urban canopy flow and the faster-moving flow aloft.

The cross-section near the church (Figure 8) highlights the region associated with the highest mean wind speeds in the domain. The location of the accelerated flow remains largely unchanged across all simulations, while the magnitude of the wind speed increases systematically with inflow velocity. This behaviour is consistent with the persistent high-wind region identified in the horizontal wind-speed distributions maps (Figure 5).

https://doi.org/10.5194/egusphere-2026-4081
Preprint. Discussion started: 4 August 2026

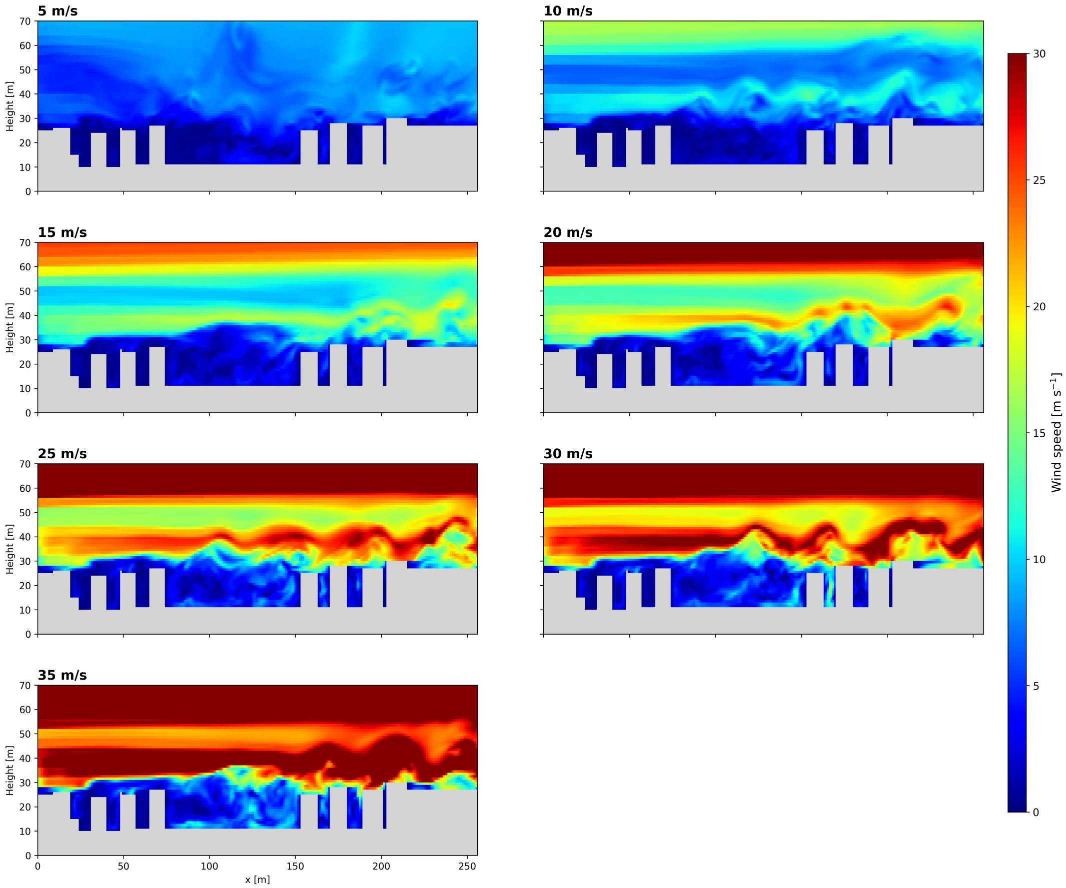

Figure 7. Snapshot of the vertical cross-section of mean wind speed for the seven model runs along the central transect shown in Figure 2, red dashed line.

Urban flow characteristic is usually described by analysing local wind speed recordings deriving statistical parameters such as the mean wind speed, turbulence intensity and gust wind speed for a sufficient number of single points. For a comprehensive assessment of how changing atmospheric boundary conditions influence the urban flow field and which consequences this might hold for wind loading and microclimate, a new approach is suggested where wind data are analysed for an individual grid level (= elevation level) and compare across the grid levels across the urban boundary layer. This approach is shown in Figure 9 on the example of occurrence distributions of 10 minutes mean wind speeds per grid level in the lower 50 m of Child 2 domain (highest resolution at target area).

First, the height at which the wind speed distribution transitions from canopy-dominated to free-stream-dominated remains stable across all inflow velocities, reinforcing the result from Figures 7 and 8 that the vertical structure of the flow is set by urban geometry rather than by the strength of the approaching wind.

https://doi.org/10.5194/egusphere-2026-4081
Preprint. Discussion started: 4 August 2026

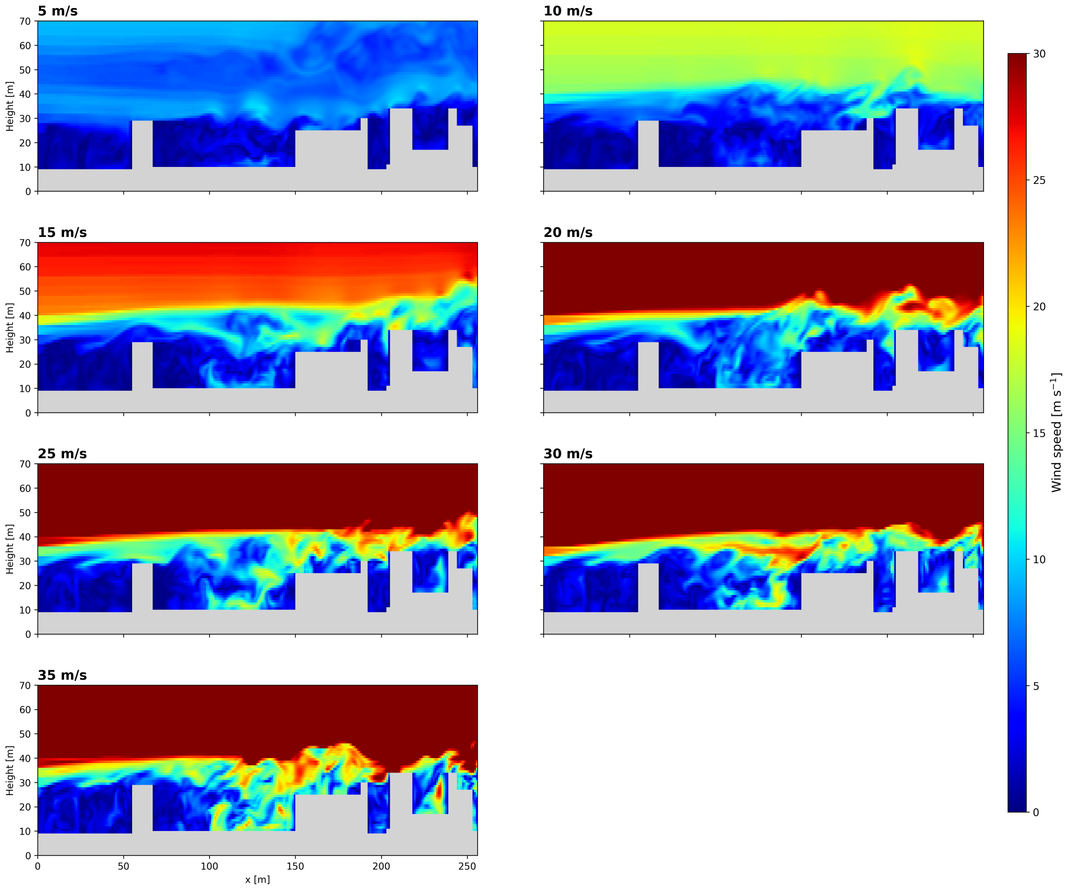

Figure 8. Snapshot of the vertical cross-section of the 10-min mean wind speed for the seven model runs along the transect near Helligåndskirken shown in Figure 2 green dotted line.

Second, while the canopy is dominated by low wind speeds at every inflow velocity, the internal spread of wind speeds within the canopy widens with increasing inflow: at low inflow (5–10 ms^{-1}), the canopy distribution is narrowly concentrated in a single low-speed bin at nearly every height, whereas at higher inflow (25–35 ms^{-1}) the canopy shows a markedly broader mixture of wind speed bins. This indicates that stronger background forcing does not simply translate into uniformly faster canopy flow, but instead increases the heterogeneity of wind exposure within the canopy itself.

Third, the maximum wind speed profile consistently exceeds the prescribed inflow profile, particularly in the upper canopy and across the transition layer, while the mean wind speed profile remains at or below the inflow profile throughout the canopy. This gap between local maximum and inflow wind speed widens in absolute terms with increasing inflow velocity, providing direct visual confirmation that the amplification of extreme local wind speeds relative to the imposed background forcing is not constant but grows with storm intensity.

https://doi.org/10.5194/egusphere-2026-4081
Preprint. Discussion started: 4 August 2026

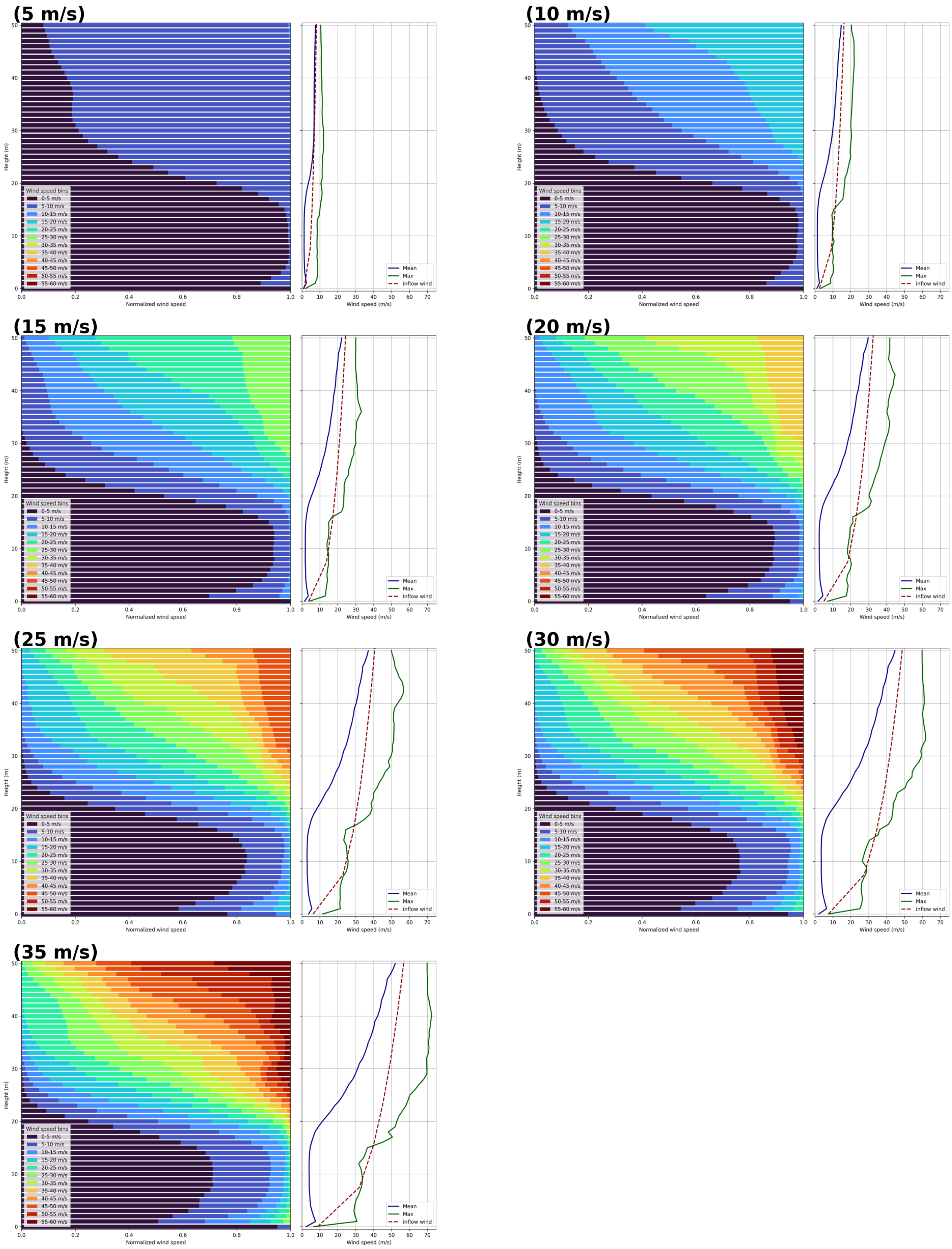

Figure 9. Normalised wind speed distributions and vertical wind profiles for the seven model runs within the lowest 50 m above ground level in the Child 2 domain. The colour-shaded distributions show the normalised wind speed occurrence, while the blue and green lines represent the mean and maximum wind speed profiles, respectively. The red dashed line indicates the corresponding inflow wind profile.

https://doi.org/10.5194/egusphere-2026-4081
Preprint. Discussion started: 4 August 2026

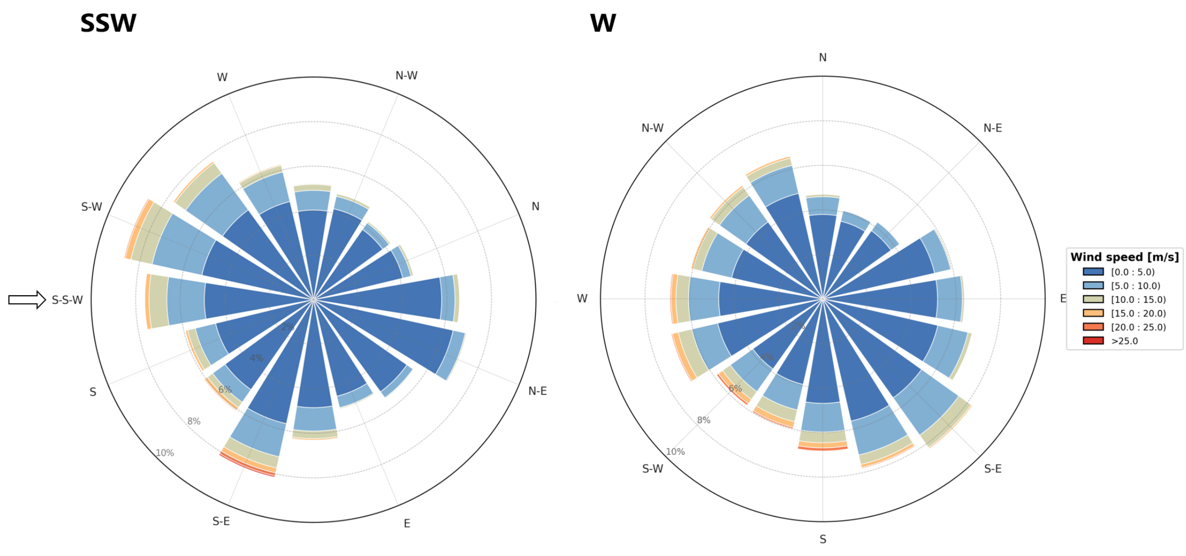

Figure 10. Distribution of wind directions within the Child 2 domain for an inflow wind speed of 25 ms^{-1} at 10 m height. The left panel shows the case with a south-southwesterly (SSW) inflow, and the right panel shows the case with a westerly (W) inflow. For comparison, the SSW case has been rotated such that the inflow direction is aligned with the westward direction.

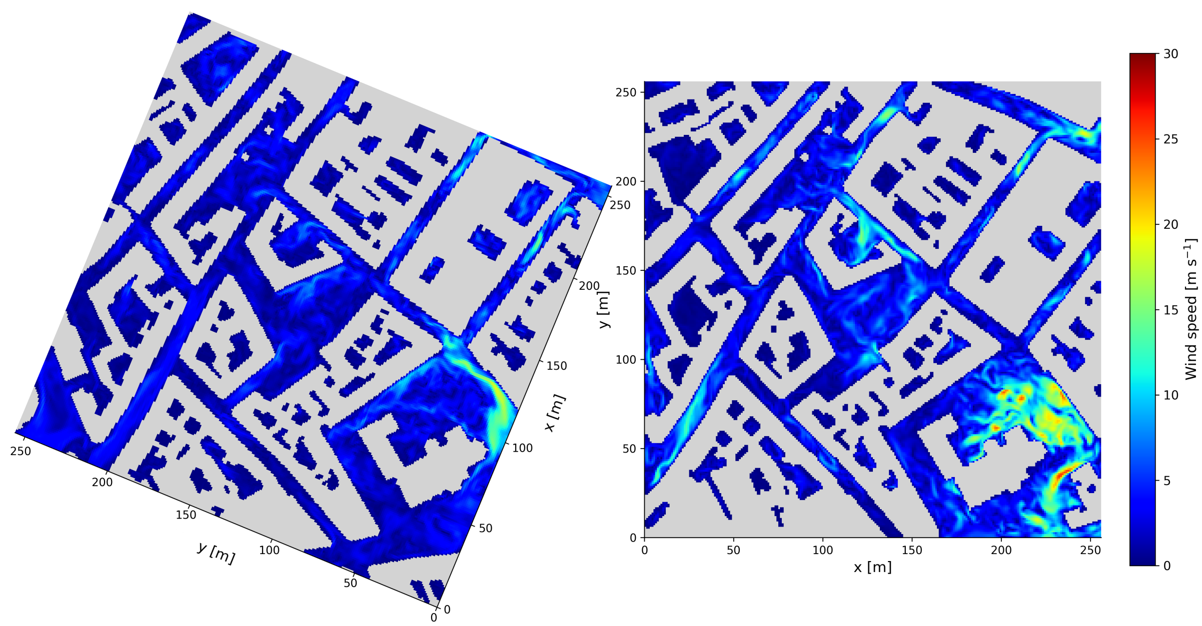

Figure 11. Spatial distribution of the 10-min mean wind speed within the Child 2 domain for an inflow wind speed of 25 ms^{-1} at 10 m height. The left panel shows the south-southwesterly (SSW) inflow case, and the right panel shows the westerly (W) inflow case. The left is rotated to show the actual orientation of the city.

https://doi.org/10.5194/egusphere-2026-4081
Preprint. Discussion started: 4 August 2026

Figure 10 compares the directional distribution of wind speed at approximately 10 m height for two inflow directions, SSW and W, testing whether the urban-geometry-controlled flow structure identified above for varying inflow magnitude also holds when the approach direction is varied. In both simulations, wind directions span nearly the full compass range despite the single prescribed inflow direction, confirming that the urban geometry substantially redirects the approaching flow through channelling and recirculation, consistent with the flow structures identified in the vertical cross-sections (Figures 7, 8).

The two inflow directions produce broadly similar overall directional distributions, but differ in which directions are associated with the highest wind speeds: for SSW inflow, the strongest winds are channelled towards directions between south and east, whereas for W inflow they are predominantly channelled towards the south. Despite this difference in channelling direction, the corresponding wind speed maps (Figure 11) show that the strongest winds in both simulations occur in the same area of the domain, in the vicinity of the church, although the specific sub-region and channelling pathway feeding this hotspot differ between the two cases. This indicates that the church area functions as a robust local wind-acceleration feature largely independent of approach direction, extending the finding, established above for varying inflow magnitude, that urban morphology controls flow structure to variation in inflow direction as well.

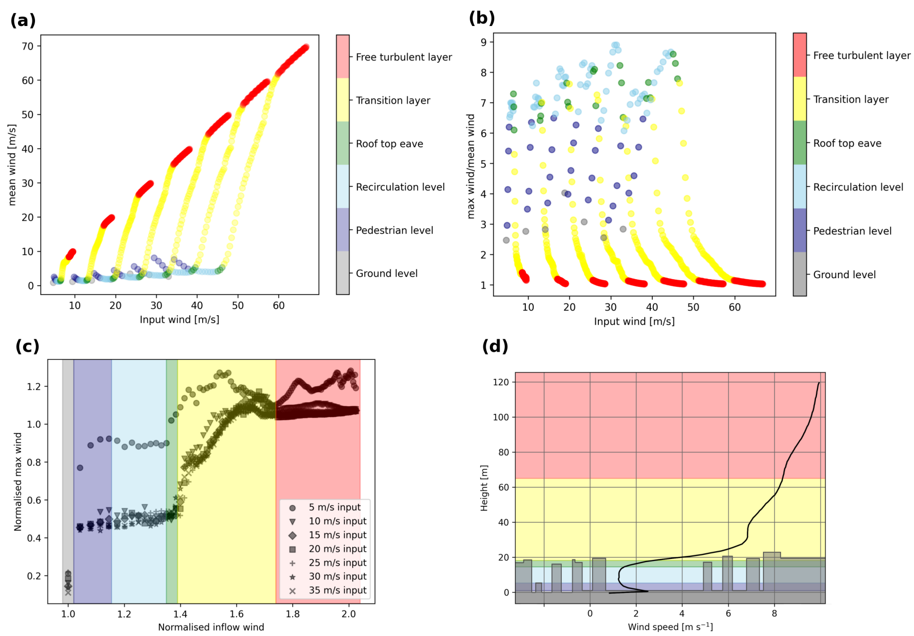

Figure 12. Relationship between inflow wind speed and simulated wind characteristics at different heights above ground level. (a) Mean wind speed as a function of inflow wind speed, indicating the urban flow respone function. (b) Ratio between maximum and mean wind speed as a function of inflow wind speed, indicating a spatial speed-up factor. (c) Normalised maximum wind speed as a function of normalised inflow wind speed. The colour scale in panels (a–c) indicates the measurement height above ground level. (d) Vertical wind profile over the urban area, with the colour scale indicating the corresponding heights above ground level.

https://doi.org/10.5194/egusphere-2026-4081
Preprint. Discussion started: 4 August 2026

An extension to the approach introduced in Figure 10 is the calculation of the grid-layer mean wind speed and its ratio to the inflow wind speed at corresponding grid height. This ratio can also be considered as a factor with which the inflow is translated into the urban flow field at a specific height. Calculating this ratio or transfer factor for all grid levels yields to a characteristics transfer factor distribution over height.

Figure 12 illustrates this calculation and the resulting transfer factor distribution with clearly identifiable features reflecting the vertical structure of the urban boundary layer. The sharpness of the distribution curve (UFT-function) allows a clear distinction between characteristic flow fields providing hence an accurate tool to observe and identify changes from varying atmospheric boundary conditions: wind speed near the ground is strongly attenuated relative to the inflow, rises through the pedestrian and recirculation layers, remains comparatively flat through the rooftop eave region, then increases sharply through the transition layer before approaching the free-stream inflow value aloft. This consistent shape across all seven inflow velocities indicates that the vertical organisation of the flow response is governed by urban morphology rather than by the magnitude of the imposed forcing, while the absolute wind speed at any given height scales with inflow velocity, the qualitative structure of the UFT-function does not.

The ratio between the domain-maximum and domain-mean wind speed (Figure 12(b)) shows a broadly consistent dependence on inflow velocity across the urban canopy. Lower inflow velocities (5–15 ms^{-1}) produce peak ratios of approximately 7–7.5, while higher inflow velocities (20–35 ms^{-1}) generally produce higher peak ratios of approximately 8–9. The 30 ms^{-1} simulation is a clear exception to this trend, with peak ratios closer to those of the 5 ms^{-1} case, no methodological difference (e.g. in inflow direction or domain configuration) distinguishes this run from the others, and the cause of this deviation is not currently understood. This metric is not a classical engineering gust factor, but it provides a useful measure of spatial amplification within the urban canopy, and the overall magnitude of the ratio, consistently well above 1 across all simulations, confirms substantial spatial heterogeneity in the wind field at every inflow velocity examined.

The normalised maximum wind speed (Figure 12(c)) shows that simulations with inflow velocities between 15 and 35 ms^{-1} collapse onto a broadly consistent curve, while the 5 ms^{-1} simulation is systematically elevated within the pedestrian and recirculation layers. This provides direct, height-resolved confirmation of the result established earlier in this section: extreme local wind speeds are disproportionately amplified, relative to the mean flow, at low inflow velocities, while this amplification diminishes as inflow velocity increases. The colour correspond to the colour-height shown in Figure 12(d).

From the virtual measurements at the centre of Greyfriar Square (red dot, Figure 1), the gust factor and turbulence intensity were calculated at approximately 10 m height for the resultant horizontal wind speed, with the gust defined as the maximum 3-second wind speed within each 10-minute window of the 1-hour simulation (see Section 2.6). Figure 13 shows an example time series, gust factor, and turbulence intensity for the 15 ms^{-1} inflow run, illustrating the high-frequency variability captured by the raw and 3-second-smoothed wind speed signals underlying these metrics.

Table 1 summarises the resulting gust factor and turbulence intensity across all seven inflow velocities. Both quantities show a clear, non-monotonic pattern with inflow velocity: high and variable values at low inflow, a rapid decline through intermediate inflow speeds, and a stable plateau at high inflow. Three regimes are identified based on this pattern, with boundaries placed at the inflow velocities where both metrics visibly shift between these behaviours: an intermittent regime (5–10 ms^{-1}), in

https://doi.org/10.5194/egusphere-2026-4081
Preprint. Discussion started: 4 August 2026

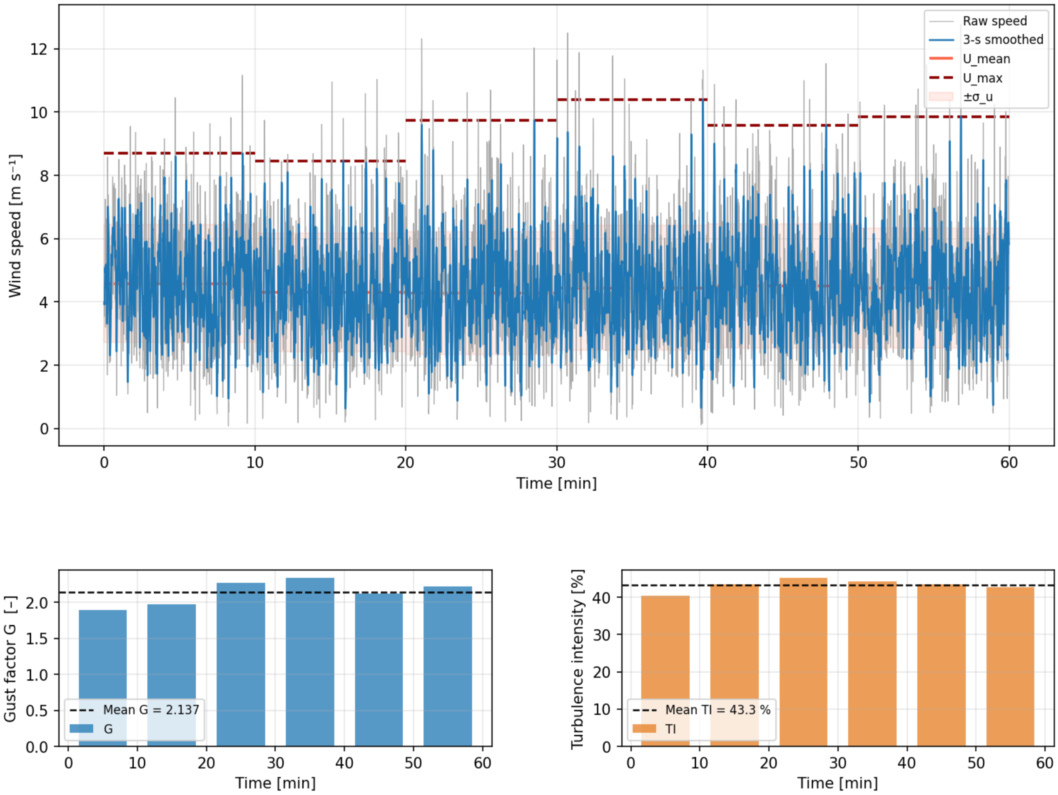

Figure 13. Time series of wind speed, gust factor, and turbulence intensity from the PALM-4U virtual measurement point located at the centre of Gråbrødretorv (red dot in Figure 1). Results are shown for an inflow wind speed of 15 ms^{-1} at 10 m height. The upper panel shows the wind speed development over a 1-hour period, while the lower panels show the corresponding gust factor and turbulence intensity calculated using a 3 s gust window and a 10 min averaging period.

which both metrics are elevated and vary substantially between runs (G = 2.55–2.60, I_U= 52–55%); a transition regime (15–20 ms^{-1}), in which both metrics fall rapidly (G = 1.81–2.14, I_U= 39–43 %); and a quasi-saturated regime (25–35 ms^{-1}), in which both metrics plateau at approximately constant values (G ≈ 1.7, I_U ≈ 40 %), varying by less than 0.1 in gust factor and 1 percentage point in turbulence intensity across this five-fold range of inflow speeds. This classification is based on visual inspection of the table values rather than a formal statistical breakpoint criterion, and is intended descriptively rather than as a precise physical threshold.

Both turbulence intensity and gust factor decrease with increasing inflow velocity at 10 m height within the urban canopy, consistent with the regime structure identified above. In the intermittent regime, flow is dominated by geometry-driven recirculation and intermittent downward turbulent penetration events: at low wind speeds the flow has less inertial dominance, so building wakes, recirculation zones, and pressure-driven channelling create relatively larger fluctuations compared to the mean. While high I_U values are well documented at pedestrian level in urban areas (Hirose et al., 2022; Zou et al., 2021), field measurements

https://doi.org/10.5194/egusphere-2026-4081
Preprint. Discussion started: 4 August 2026

Table 1. Summary of wind characteristics for all model runs, including mean and maximum wind speed, gust factor, and turbulence intensity (I_U). The identified flow regimes are indicated by colour: blue represents intermittent flow, teal represents the transition regime, and green represents quasi-saturated flow.

		Windspeed [ms^{-1}]			Gust factor			Turbulence intensity [%]		
Regime	**model run**	$\bar{u}$	σ_u	u_{max}	mean	min	max	mean	min	max
Intermittent	5 ms^{-1}	1.94	1.07	4.93	2.55	2.21	2.82	55.2	49.5	61.4
	10 ms^{-1}	2.30	1.21	5.96	2.60	2.46	2.81	52.2	51.8	55.4
Transition	15 ms^{-1}	4.43	1.91	9.46	2.14	1.90	2.27	43.3	40.5	45.1
	20 ms^{-1}	5.55	2.15	10.06	1.81	1.69	1.91	38.8	37.9	41.4
Quasi-saturated	25 ms^{-1}	6.80	2.70	11.87	1.74	1.71	1.81	39.6	39.1	41.0
	30 ms^{-1}	7.97	3.19	13.61	1.71	1.65	1.79	40.0	39.1	41.7
	35 ms^{-1}	9.29	3.70	15.61	1.68	1.61	1.77	39.9	38.3	40.7

at 10 m height in urban settings also report a wide I_U range, depending on wind direction and local geometry (Zou et al., 2021). The gust factors observed here are high but physically plausible for a street canyon at this height.

As inflow increases through the transition regime, the urban canopy becomes increasingly ventilated, leading to a more continuous mean flow and a relative reduction in velocity fluctuations. In the quasi-saturated regime, both metrics approach asymptotic values, indicating a transition to a turbulence regime governed primarily by urban shear-layer dynamics rather than inflow intermittency. At 10 m height in a dense urban environment, the turbulence intensity in the quasi-saturated regime is at the high end of the expected range, but physically plausible. Field measurements within urban street canyons report I_U between 25–50%, with the spread driven by building density, canyon geometry, and measurement position (Eliasson et al., 2006; Rotach, 1995). Locations near building wakes or within sheltered recirculation zones consistently produce values at the upper bound. For context, the IEC wind turbine standard classifies $I_U \approx 16\%$ as turbulence class A ("high turbulence") (Hansen and Larsen, 2005); urban canopies routinely exceed this by a factor of two or more.

Davenport (1967) and later Wiernga (1993) and Rakib et al. (2020) give gust factors for urban terrain of roughly 1.6–1.9 for 10 m height and 10-minute means, within which the quasi-saturated plateau sits squarely. The elevated values in the intermittent regime are consistent with the well-established behaviour of gust factor decreasing with increasing mean wind speed, documented across urban measurement studies and LES (Davis and Newstein, 1968; Hirose et al., 2022).

4 Discussion

This study examines how imposed inflow wind forcing translates into urban-scale wind exposure using high-resolution LES with PALM-4U, focusing on the governing physical mechanisms and their implications for urban wind hazards under climate change, as a step toward the longer-term goal of linking large-scale storm intensity to local urban wind hazard.

https://doi.org/10.5194/egusphere-2026-4081
Preprint. Discussion started: 4 August 2026

The persistence of the spatial wind-speed patterns across all simulations indicates that urban morphology is the primary control on flow organisation. Local acceleration zones consistently occur in the open area near the church and in streets aligned with the inflow direction, reflecting combined effects of channelling and geometric flow steering. These features remain stable across inflow magnitudes, indicating that inflow forcing primarily modulates intensity rather than spatial structure.

The enhanced velocities near the church are likely linked to local flow acceleration induced by the building geometry and surrounding open space. While the model representation of the church is simplified and does not resolve the full tower structure, the persistent acceleration in this region suggests that combined effects of geometry and upstream flow deflection contribute to momentum concentration downstream.

The differing timing of domain-maximum wind-speed peaks (Figure 6) underscores that, subject to the single-realisation caveat noted there, peak velocities are governed by transient turbulent structures distinct from the morphology- and inflow-controlled mean flow. Extreme winds therefore cannot be assumed to scale directly with mean flow conditions.

Vertical cross-sections confirm this pattern, showing consistent rooftop shear-layer formation and persistent high-velocity zones near the church across all runs. The rooftop shear layer marks the transition between canopy-dominated and overlying atmospheric flow, where velocity gradients are strongest.

The relationship between inflow velocity and simulated wind response shows near-linear scaling for domain-averaged quantities ($R^2 = 0.99$), with the domain-maximum wind speed scaling at approximately 8.5 times the rate of the domain mean (Appendix C), while maintaining consistent vertical structure across all cases. Deviations occur primarily in extreme values, where normalised maxima indicate non-linear behaviour under weak inflow conditions. Above the urban canopy, wind speeds converge toward a linear response, suggesting diminishing influence of urban drag with height.

Vertical wind-speed distributions demonstrate a stable structural separation between the urban canopy and the overlying atmospheric flow, consistent with the urban flow transfer function (UFT-function) identified across all inflow velocities. Within the canopy, momentum is reduced by building-induced drag, producing persistently low wind speeds up to rooftop height; within the urbansphere transition layer above, wind speed increases rapidly and scales more directly with inflow conditions.

Despite a fixed inflow direction, the urban canopy produces a wide distribution of local wind directions due to channelling, separation, and recirculation within the street network. While directional spreading is similar for both SSW and W inflow cases, the strongest winds remain consistently associated with the vicinity of the church, although their directional characteristics vary depending on inflow orientation. Combined with the directional independence of the high-wind region's location, and its consistency across the full range of inflow magnitudes examined, this demonstrates that the church area's role as a local wind-acceleration feature is governed by urban morphology along two largely independent axes of variation, inflow speed and inflow direction, rather than being an artefact specific to either. This decouples the spatial pattern of near-surface extreme winds from the direction of large-scale atmospheric forcing, though the present analysis covers only two inflow directions and should not be taken as exhaustive across all possible approach angles.

Greyfriar Square functions as a roughness transition zone where flow from surrounding street canyons interacts with a relatively open square. This configuration promotes shear-layer formation at the interface between incoming channelled flows and the open space, resulting in intermittent momentum exchange and enhanced turbulence levels at measurement height. It is

https://doi.org/10.5194/egusphere-2026-4081
Preprint. Discussion started: 4 August 2026

noted, however, that turbulence appears more developed in the eastern portion of the domain in vertical cross-sections, which may partly reflect the influence of the coarser nesting interface upstream rather than purely local flow physics.

The child domain nesting employs a refinement ratio of 8:4:1, with the innermost domain at 1 m grid spacing nested within a 4 m intermediate domain, itself nested within the 8 m parent domain. The ratio between the two innermost domains (4:1) is at the upper edge of the range of 2–4 typically recommended to minimise interpolation errors at the nesting interface (Hellsten et al., 2021). Vertical cross-sections of turbulence quantities show a visible asymmetry, with turbulence appearing more fully developed in the downstream portion of the domain. While this pattern is broadly consistent with the physical development of a shear layer across the open square, it may also partly reflect numerical diffusion or interpolation errors introduced at the upstream nesting boundary. A formal grid independence study, varying grid resolution and nesting ratio systematically, would be required to fully separate these contributions, and is identified as a priority for future work. The analysis and conclusions of the present study are based on domain-averaged and spatially aggregated quantities that are less sensitive to localised near-boundary artefacts, but localised point measurements near the upstream nesting interface should be interpreted with this caveat in mind.

Three flow regimes emerge across increasing inflow velocities, identified from the visible pattern of gust factor and turbulence intensity values rather than a formal statistical breakpoint criterion (see Results): an intermittent regime (5–10 m s^{-1}), in which flow is dominated by intermittent recirculation and penetration events, producing elevated gust factors and turbulence intensity; a transition regime (15–20 m s^{-1}), in which increasing momentum reduces the dominance of cavity-scale circulation; and a quasi-saturated regime (25–35 m s^{-1}), in which both turbulence intensity and gust factor approach quasi-stationary values, indicating a shear-dominated equilibrium governed by persistent canopy-layer mixing.

The results highlight the importance of distinguishing between mean and gust-related wind exposure in urban environments. At low inflow velocities, intermittent gust penetration leads to disproportionately high gust factors, whereas at higher wind speeds the relationship between mean and peak flow stabilises. Despite this stabilisation, turbulence levels remain high, indicating persistent unsteadiness relevant for pedestrian exposure.

5 Conclusion

Regarding the first research question, this study demonstrates how progressively intensified inflow wind forcing translates into urban-scale wind exposure in a dense historical district of central Copenhagen.

To assess influence from changing atmospheric boundary conditions on the urban wind field, a new approach of analysing and presenting characteristic parameters of the urban flow has been suggested. Here, the comparison of flow transfer functions (UFT-function) allows a very clear identification of consequences for the flow field.

Across the full range of inflow velocities examined, from gentle breeze to hurricane-force wind, the spatial structure of the flow, remains largely invariant, indicating that urban morphology governs the organisation of the wind field, while inflow magnitude primarily acts as a scaling factor for mean wind conditions. Regarding the second research question, extreme wind behaviour instead exhibits clear regime-dependent behaviour, with the intermittent, transition, and quasi-saturated regimes

https://doi.org/10.5194/egusphere-2026-4081
Preprint. Discussion started: 4 August 2026

identified above: at low inflow velocities, gustiness is strongly amplified by intermittent, geometry-driven recirculation processes, whereas at higher wind speeds both turbulence intensity and gust factors converge toward quasi-stationary values characteristic of a shear-dominated canopy flow regime.

These results indicate that urban wind hazards under intensified storm conditions cannot be inferred from mean wind scaling alone, as gust amplification is governed by non-linear interactions between turbulent structures and urban geometry that are most pronounced at low-to-moderate inflow velocities, and diminish as the flow transitions to the shear-dominated quasi-saturated regime at higher wind speeds. The study therefore provides a physically based framework for understanding how changes in inflow wind intensity map to local wind hazard metrics in complex urban environments, explicitly distinguishing between mean-flow scaling and turbulence-driven extremes, as a foundation for future work linking this framework to large-scale storm forcing.

Regarding the third research question, the simulations show internally consistent, physically plausible behaviour across the full seven-fold range of inflow forcing, near-linear mean-flow scaling (R^2 = 0.99), a stable vertical flow structure, and gust factors and turbulence intensities consistent with published urban measurements (Davenport, 1967; Wiernga, 1993; Rakib et al., 2020), supporting the use of PALM-4U for urban wind hazard assessment under storm conditions. This support remains provisional given the limited independent validation data (Section 2.5) and the unresolved sensitivity to the 4:1 nesting ratio (Section 2.7 and 4), both identified as priorities for future work.

Overall, the findings highlight the importance of explicitly resolving urban-scale turbulence when assessing future wind hazards under climate-induced storm intensification. These results are particularly relevant for translating projected changes in storm intensity into spatially resolved urban wind risk under climate change.

6 Code and data availability.

The Palm-4u model is freely available at https://palm.muk.uni-hannover.de (Last access: 07.04.2026). The LES performed and used in this article where performed with Palm-4u v24.04. The model set up can be required by author.

https://doi.org/10.5194/egusphere-2026-4081
Preprint. Discussion started: 4 August 2026

Appendix A: Model Domain and Nesting Configuration

The nested domain configuration used in the PALM-4U simulations is displayed in Figure A1 and summarized in Table A1. The model setup consists of a parent domain and two nested child domains with progressively higher spatial resolution in order to resolve flow structures within the urban area of interest. The table lists the horizontal domain extents and corresponding grid spacings for each model domain.

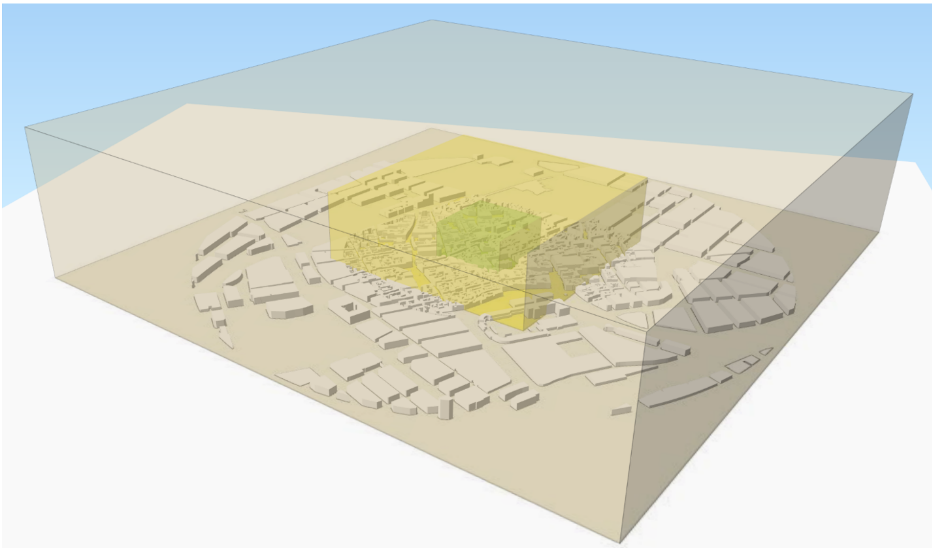

Figure A1. 3D visualization of the computational parent domain (grey), and nested sub-domains; child 1 (yellow) and child 2 (green).

Table A1. Domain and grid extensions of parent and nested sub-domains of the computational domain.

	Palm-4u Model		
	parent	child 1	child 2
number of gridboxes in:			
x	256	192	256
y	256	192	256
z	64	64	128
size [m] of single gridbox in:			
x	8.0	4.0	1.0
y	8.0	4.0	1.0
z	8.0	4.0	1.0

https://doi.org/10.5194/egusphere-2026-4081
Preprint. Discussion started: 4 August 2026

Appendix B: Topography Model

This study employs an existing PALM topography model (static driver) developed as part of an investigation of urban microclimate analysis and the bio-meteorological capabilities of PALM-4U (Jensen, 2025). A step-wise refinement of the urban architectural detailing (based on building footprint and building height variations) was applied toward the central area of interest, while buildings near the domain periphery were represented as simplified massing blocks. Due to limitations in PALM's inflow boundary conditions, the model setup was designed inspired by principles of a wind tunnel turntable configuration, with the urban geometry centred on a disc. This approach enabled the assessment of varying wind directions while minimizing the need for modifications to the computational model.

Figure B1 displays the differentiation between surface types in the model which use different PALM bulk material properties. This characterization was based on data availability of the area, and contributed to some simplified representations of the urban environment, e.g. the model assumes homogeneous building facade properties. Other simplifications follow from PALM's Cartesian grid structure e.g. flat roofs.

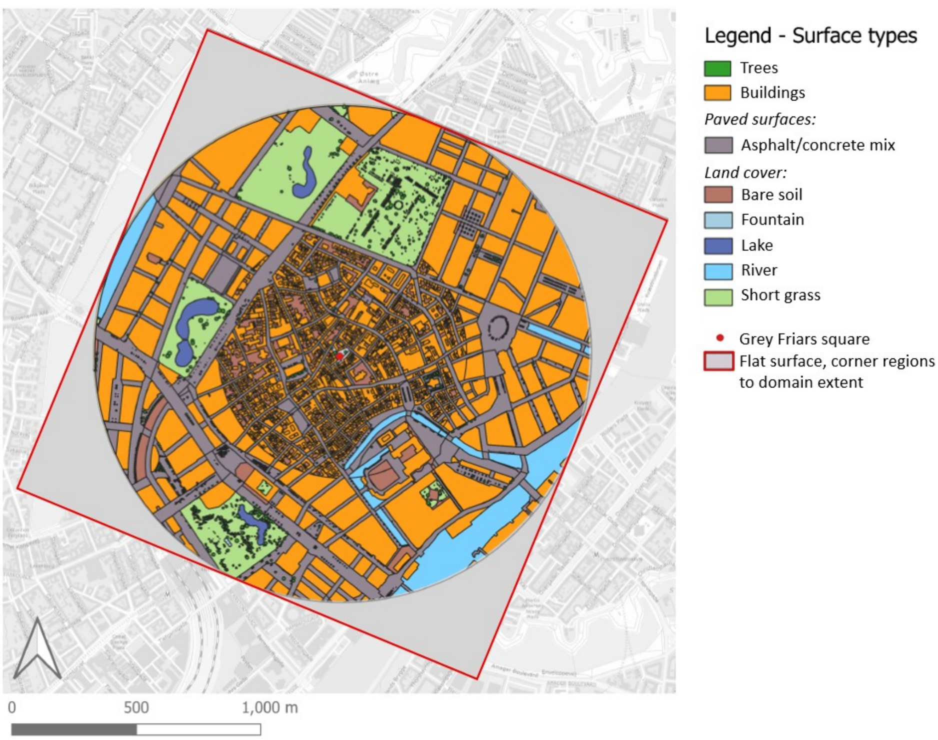

Figure B1. Surface layers of the topography model included in the PALM static driver. (Illustration modified from Jensen (2025)).

https://doi.org/10.5194/egusphere-2026-4081
Preprint. Discussion started: 4 August 2026

Appendix C: Mean and max wind vs inflow scaling

475 The domain-averaged (a) and domain-maximum (b) wind speed at 10 m height within Child 2 as a function of the imposed inflow wind speed, for all seven inflow scenarios are shown in figure C1. Dashed lines show the least-squares linear fit; fit equation and coefficient of determination (R^2) are given in each panel. Both quantities scale approximately linearly with inflow wind speed, with the domain-maximum wind speed increasing at approximately 8.5 times the rate of the domain-mean (slope of 0.803 vs. 0.095 per ms^{-1} increase in inflow).

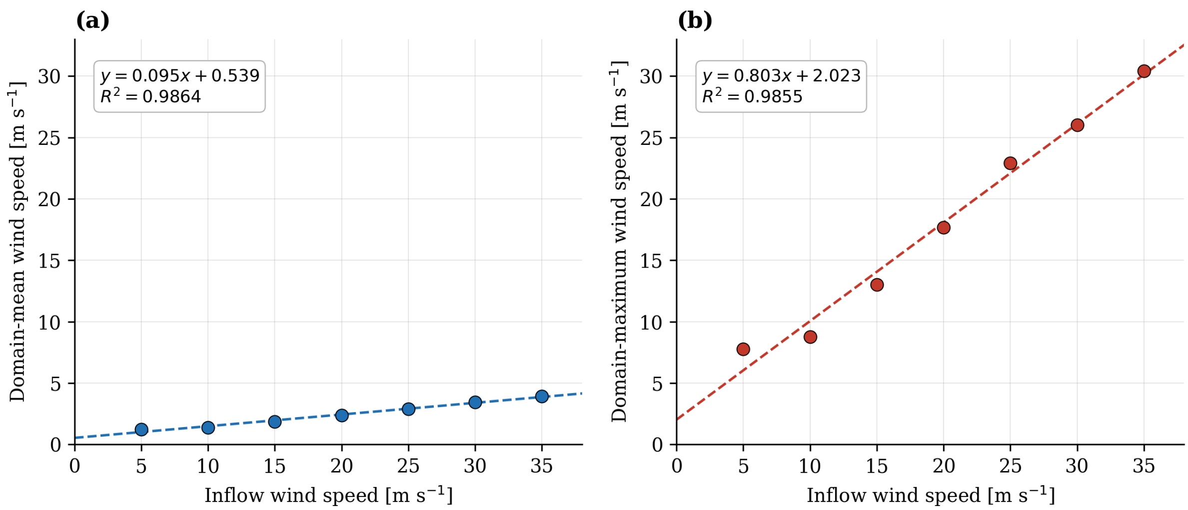

Figure C1. Domain-averaged (a) and domain-maximum (b) wind speed at 10 m height within Child 2 as a function of inflow wind speed. Dashed lines show the linear least-squares fit, with fit equation and R^2 given per panel.

https://doi.org/10.5194/egusphere-2026-4081
Preprint. Discussion started: 4 August 2026

Author contribution

JKHØ: PALM-4U model build-up/run, Formal analysis, Writing original draft, Investigation, conceptualization. JHC: Conceptualization, Review/editing. ARHJ: PALM-4U model build-up, review/editing. HHHK: Conceptualization, review/editing.

Competing interests

The authors declare that they have no conflict of interest.

Acknowledgements

This work was supported by the Realdania Philanthropy project PRJ-2021-00176 "Metoder til klimatilpasning af det byggede miljø". JKHØ acknowledge the support of the Danish government through the National Center for Climate Research (NCKF) Artificial intelligence tools were used to assist in improving the clarity and wording of parts of the manuscript. All content was reviewed and verified by the authors. The authors would like to thank DTU compute for the use of their HPC cluster and support.

https://doi.org/10.5194/egusphere-2026-4081
Preprint. Discussion started: 4 August 2026

References

Belda, M., Resler, J., Geletič, J., Krč, P., Maronga, B., Sühring, M., Kurppa, M., Kanani-Sühring, F., Fuka, V., Eben, K., Benešová, N., and Auvinen, M.: Sensitivity analysis of the PALM model system 6.0 in the urban environment, Geoscientific Model Development, 14, 4443–4464, https://doi.org/10.5194/gmd-14-4443-2021, 2021.

Blocken, B.: Computational Fluid Dynamics for urban physics: Importance, scales, possibilities, limitations and ten tips and tricks towards accurate and reliable simulations, Building and Environment, 91, 219–245, https://doi.org/https://doi.org/10.1016/j.buildenv.2015.02.015, fifty Year Anniversary for Building and Environment, 2015.

Bramsen, B. and Fogtdal, P.: København før og nu - og aldrig, Palle Fogtdal, 1997.

Büeler, D. and Pfahl, S.: Potential Vorticity Diagnostics to Quantify Effects of Latent Heating in Extratropical Cyclones. Part I: Methodology, Journal of the Atmospheric Sciences, 74, 3567–3590, https://doi.org/10.1175/JAS-D-17-0041.1, 2017.

Catto, J. L.: Extratropical cyclone classification and its use in climate studies, Reviews of Geophysics, 54, 486–520, https://doi.org/https://doi.org/10.1002/2016RG000519, 2016.

Catto, J. L., Ackerley, D., and Booth, J. e. a.: The Future of Midlatitude Cyclones., Current Climate Change Reports, 5, https://doi.org/https://doi.org/10.1007/s40641-019-00149-4, 2019.

Davenport, A.: Gust loading factors, Journal of the Structural Division, 93, 11–34, 1967.

Davis, F. K. and Newstein, H.: The Variation of Gust Factors with Mean Wind Speed and with Height, Journal of Applied Meteorology and Climatology, 7, 372 – 378, https://doi.org/10.1175/1520-0450(1968)007<0372:TVOGFW>2.0.CO;2, 1968.

Eliasson, I., Offerle, B., Grimmond, C., and Lindqvist, S.: Wind fields and turbulence statistics in an urban street canyon, Atmospheric Environment, 40, 1–16, https://doi.org/https://doi.org/10.1016/j.atmosenv.2005.03.031, 2006.

Ermis, S., Leach, N. J., Lott, F. C., Sparrow, S. N., and Weisheimer, A.: Event attribution of a midlatitude windstorm using ensemble weather forecasts, Environmental research: Climate, 3, https://doi.org/10.1088/2752-5295/ad4200, 2024.

Fernando, H. J. S.: Fluid dynamics of urban atmospheres in complex terrain, Annual Review of Fluid Mechanics, 42, 365–389, 2010.

Hansen, K. and Larsen, G. C.: Characterising turbulence intensity for fatigue load analysis of wind turbines., Wind Engineering, 29, 319–329, https://doi.org/10.1260/030952405774857897, 2005.

Hawkins, E., Compo, G. P., and Sardeshmukh, P. D.: ESD Ideas: Translating historical extreme weather events into a warmer world, Earth System Dynamics, 14, 1081–1084, https://doi.org/10.5194/esd-14-1081-2023, 2023.

Hellsten, A., Ketelsen, K., Sühring, M., Auvinen, M., Maronga, B., Knigge, C., Barmpas, F., Tsegas, G., Moussiopoulos, N., and Raasch, S.: A nested multi-scale system implemented in the large-eddy simulation model PALM model system 6.0, Geoscientific Model Development, 14, 3185–3214, https://doi.org/10.5194/gmd-14-3185-2021, 2021.

Hirose, C., Nomichi, T., and Ikegaya, N.: Distributions of gust and peak factors at a pedestrian level in a simplified urban canopy obtained by particle image velocimetry, Building and Environment, 222, 109 350, https://doi.org/https://doi.org/10.1016/j.buildenv.2022.109350, 2022.

Hoskins, B. J. and Hodges, K. I.: New Perspectives on the Northern Hemisphere Winter Storm Tracks, Journal of the Atmospheric Sciences, 59, 1041 – 1061, https://doi.org/10.1175/1520-0469(2002)059<1041:NPOTNH>2.0.CO;2, 2002.

IPCC: Climate Change 2021: The Physical Science Basis. Contribution of Working Group I to the Sixth Assessment Report of the Intergovernmental Panel on Climate Change. Edited by Masson-Delmotte, V. and Zhai, P. and Pirani, A. and Connors, S. L. and Péan, C. and Berger, S. and Caud, N. and Chen, Y. and Goldfarb, L. and Gomis, M. I. and Huang, M. and Leitzell, K. and Lonnoy, E. and Matthews,

J. B. R. and Maycock, T. K. and Waterfield, T. and Yelekçi, O. and Yu, R. and Zhou, B., Cambridge University Press, Cambridge, United Kingdom and New York, NY, USA, https://doi.org/10.1017/9781009157896, 2021.

IPCC: Climate Change 2022: Impacts, Adaptation, and Vulnerability. Contribution of Working Group II to the Sixth Assessment Report of the Intergovernmental Panel on Climate Change. Edited by Pörtner, H.-O. and Roberts, D. C. and Tignor, M. and Poloczanska, E. S. and Mintenbeck, K. and Alegría, A. and Craig, M. and Langsdorf, S. and Löschke, S. and Möller, V. and Okem, A. and Rama, B., Cambridge University Press, Cambridge, United Kingdom and New York, NY, USA, https://doi.org/10.1017/9781009325844, 2022.

Jensen, A. R. H.: Sensitivity Study of Urban Microclimate to Environmental Variations, Master's thesis, DTU Department of Civil and Mechanical Engineering, master's Thesis, 2025.

Jensen, A. R. H. and Koss, H. H.: Validation of UTCI simulation with PALM-4U on direct measurements in urban environments, unpublished at the time of this paper., 2026.

Kiseleva, O., Gantner, L., Kalthoff, N., Kossmann, M., and Holst, C.: Evaluation of the Urban Climate Model PALM-4U over Hilly Terrain Using Wind and Turbulence Observations, Meteorologische Zeitschrift, 33, 177–198, https://doi.org/10.1127/metz/2024/1193, 2024.

Maronga, B., Banzhaf, S., Burmeister, C., Esch, T., Forkel, R., Fröhlich, D., Fuka, V., Gehrke, K. F., Geletič, J., Giersch, S., Gronemeier, T., Groß, G., Heldens, W., Hellsten, A., Hoffmann, F., Inagaki, A., Kadasch, E., Kanani-Sühring, F., Ketelsen, K., Khan, B. A., Knigge, C., Knoop, H., Krč, P., Kurppa, M., Maamari, H., Matzarakis, A., Mauder, M., Pallasch, M., Pavlik, D., Pfafferott, J., Resler, J., Rissmann, S., Russo, E., Salim, M., Schrempf, M., Schwenkel, J., Seckmeyer, G., Schubert, S., Sühring, M., von Tils, R., Vollmer, L., Ward, S., Witha, B., Wurps, H., Zeidler, J., and Raasch, S.: Overview of the PALM model system 6.0, Geoscientific Model Development, 13, 1335–1372, https://doi.org/10.5194/gmd-13-1335-2020, 2020.

Nazarian, N., Krayenhoff, E. S., and Martilli, A.: A one-dimensional model of turbulent flow through "urban" canopies (MLUCM v2.0): updates based on large-eddy simulation, Geoscientific Model Development, 13, 937–953, https://doi.org/10.5194/gmd-13-937-2020, 2020.

Oke, T.: Methods in urban climatology, Applied Climatology, 14, 19–29, 1984.

Priestley, M. D. K. and Catto, J. L.: Future changes in the extratropical storm tracks and cyclone intensity, wind speed, and structure, Weather and Climate Dynamics, 3, 337–360, https://doi.org/10.5194/wcd-3-337-2022, 2022.

Priestley, M. D. K., Stephenson, D. B., Scaife, A. A., Bannister, D., Allen, C. J. T., and Wilkie, D.: Forced trends and internal variability in climate change projections of extreme European windstorm frequency and severity, Quarterly Journal of the Royal Meteorological Society, 150, 4933–4950, https://doi.org/https://doi.org/10.1002/qj.4849, 2024.

Rakib, M., Evans, S., and Clausen, P.: Measured gust events in the urban environment, a comparison with the IEC standard, Renewable Energy, 146, 1134–1142, https://doi.org/https://doi.org/10.1016/j.renene.2019.07.058, 2020.

Resler, J., Eben, K., Geletič, J., Krč, P., Rosecký, M., Sühring, M., Belda, M., Fuka, V., Halenka, T., Huszár, P., Karlický, J., Benešová, N., Ďoubalová, J., Honzáková, K., Keder, J., Nápravníková, v., and Vlček, O.: Validation of the PALM model system 6.0 in a real urban environment: a case study in Dejvice, Prague, the Czech Republic, Geoscientific Model Development, 14, 4797–4842, https://doi.org/10.5194/gmd-14-4797-2021, 2021.

Resler, J., Bauerová, P., Belda, M., Bureš, M., Eben, K., Fuka, V., Geletič, J., Jareš, R., Karel, J., Keder, J., Krč, P., Patiño, W., Radović, J., Řezníček, H., Sühring, M., Šindelářová, A., and Vlček, O.: Challenges of high-fidelity air quality modeling in urban environments – PALM sensitivity study during stable conditions, Geoscientific Model Development, 17, 7513–7537, https://doi.org/10.5194/gmd-17-7513-2024, 2024.

Rotach, M.: Profiles of turbulence statistics in and above an urban street canyon, Atmospheric Environment, 29, 1473–1486, https://doi.org/https://doi.org/10.1016/1352-2310(95)00084-C, 1995.

https://doi.org/10.5194/egusphere-2026-4081
Preprint. Discussion started: 4 August 2026

Thordal, M. S., Bennetsen, J. C., Capra, S., and Koss, H. H. H.: Towards a standard CFD setup for wind load assessment of high-rise buildings: Part 1 – Benchmark of the CAARC building, Journal of Wind Engineering and Industrial Aerodynamics, 205, 104 283, https://doi.org/https://doi.org/10.1016/j.jweia.2020.104283, 2020.

Ulbrich, U., Leckebusch, G., and Pinto, J. G.: Extra-tropical cyclones in the present and future climate: a review, Theoretical and Applied Climatology, 96, https://doi.org/10.1007/s00704-008-0083-8, 2009.

Wiernga, J.: Representative roughness parameters for homogeneous terrain, Boundary-Layer Meteorology, 63, 1573–1472, https://doi.org/10.1007/BF00705357, 1993.

Zeitzen, R. M. K., Christensen, J. H., Øelund, J. K. H., Feddersen, H., Vedel, H., Nielsen, N. W., and Matte, D.: Windstorm Extremes in a Warmer World: Raising the Bar for Destruction., Geophysical Research Letters, 52, https://doi.org/10.1029/2025GL115936, 2025.

Zou, J., Yu, Y., Liu, J., Niu, J., Chauhan, K., and Lei, C.: Field measurement of the urban pedestrian level wind turbulence, Building and Environment, 194, 107 713, https://doi.org/https://doi.org/10.1016/j.buildenv.2021.107713, 2021.

Øelund, J. K. H., Christensen, J. H., Zeitzen, R. M. K., Vedel, H., and Feddersen, H.: Assessing the intensification and impact of a historical storm in a warmer climate, Natural Hazards and Earth System Sciences, 26, 1039–1057, https://doi.org/10.5194/nhess-26-1039-2026, 2026.